Thermal stability of MnBi magnetic materials

J Cui[1,2]**, J P Choi**[1]**, G Li**[1]**, E Polikarpov**[1]**, J Darsell**[1]**, N Overman**[1]**, M Olszta**[1]**,
D Schreiber**[1]**, M Bowden**[3]**, T Droubay**[4]**, M J Kramer**[5,6]**, N A Zarkevich**[5]**,
L L Wang**[5]**, D D Johnson**[5,6]**, M Marinescu**[7]**, I Takeuchi**[2]**, Q Z Huang**[8]**, H Wu**[2,8]**,
H Reeve**[9]**, N V Vuong**[10]** and J P Liu**[10]

[1] Energy and Environment Directorate, Pacific Northwest National Laboratory, Richland, WA 99354, USA

[2] Department of Materials Science and Engineering, University of Maryland, College Park, MD 20742, USA

[3] Interface Spectroscopy and Diffraction, Environmental Molecular Sciences Laboratory, Richland,
WA 99354, USA

[4] Fundamental and Computational Sciences Directorate, Pacific Northwest National Laboratory, Richland,
WA 99354, USA

[5] Division of Materials Science and Engineering, Ames Laboratory/US Department of Energy, Ames,
IA 50011, USA

[6] Department of Materials Science and Engineering, Iowa State University, Ames, IA 50011, USA

[7] Electron Energy Corporation, Landisville, PA 17538, USA

[8] NIST Center for Neutron Research, National Institute of Standards and Technology, Gaithersburg,
MD 20899-6102, USA

[9] United Technologies Research Center, East Harford, CT 06108, USA

[10] Department of Physics, University of Texas at Arlington, TX 76019, USA

E-mail: jun.cui@pnnl.gov

Abstract

MnBi has attracted much attention in recent years due to its potential as a rare-earth-free permanent
magnet material. It is unique because its coercivity increases with increasing temperature, which
makes it a good hard phase material for exchange coupling nanocomposite magnets. MnBi phase is
difficult to obtain, partly because the reaction between Mn and Bi is peritectic, and partly because
Mn reacts readily with oxygen. MnO formation is irreversible and harmful to magnet performance.
In this paper, we report our efforts toward developing MnBi permanent magnets. To date, high
purity MnBi (>90%) can be routinely produced in large quantities. The produced powder exhibits
74.6 emu g^{-1} saturation magnetization at room temperature with 9 T applied field. After proper
alignment, the maximum energy product $(BH)_{max}$ of the powder reached 11.9 MGOe, and that of
the sintered bulk magnet reached 7.8 MGOe at room temperature. A comprehensive study of
thermal stability shows that MnBi powder is stable up to 473 K in air.

(Some figures may appear in colour only in the online journal)

1. Introduction

MnBi is an attractive alternative to the permanent magnets
containing rare earth elements, especially the ones for medium
temperature applications (423–473 K) such as Nd–Fe–B–Dy
and Sm–Co. MnBi has attractive temperature properties:
its coercivity increases with increasing temperature, reaching a maximum of 2.6 T at 523 K [1–4]. The high coercivity is attributed to MnBi's large magnetocrystalline
anisotropy (1.6×10^6 J m^{-3}) [5]. MnBi has relatively low
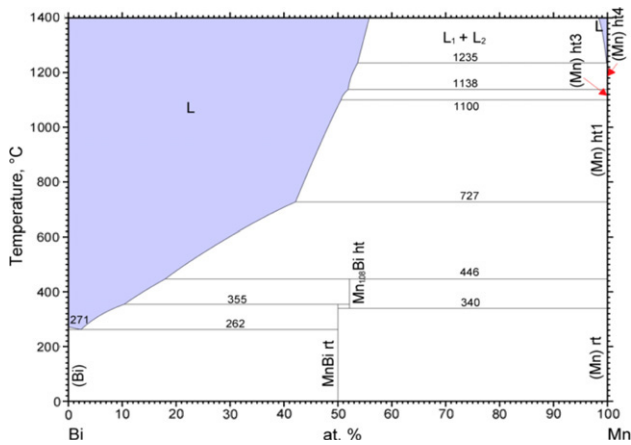
Figure 1. Mn–Bi phase diagram. Reprinted with permission of ASM International. www.asminternational.org.

magnetization. Its room temperature saturation magnetization is about 75 emu g^{-1} or 8.4 kG with 5 T field [6]. The corresponding maximum theoretical energy product (BH)$_{max}$ = $M_s^2/4$ is about 17.6 MGOe assuming the MH curve is perfectly square. In practice, single phase MnBi should exceed 10 MGOe, which is competitive compared to magnets such as ferrite and Alnico, but is only a fraction of what Nd–Fe–B and Sm–Co based magnets can offer at room temperature. To best utilize MnBi's unique high temperature properties, MnBi should be used as a hard phase to be exchange-coupled with a soft phase, so that the remanent magnetization can be improved to >1 T while coercivity is maintained at >10 kOe. The corresponding (BH)$_{max}$ entitlement is 25 MGOe.

The roadmap for developing a MnBi based exchange-coupled magnet starts with preparing high purity MnBi compound in large quantities. Synthesizing MnBi is a challenge. As shown by the Mn–Bi phase diagram [7] in figure 1, the melting temperatures of Mn and Bi are 1519 K (1246 °C) and 544 K (271 °C), respectively. A rather drastic peritectic reaction exists over wide temperature and composition ranges. Several methods have been utilized in preparation of high purity MnBi single phase, including arc-melting, sintering, and melt-spin rapid solidification [4, 8–11]. Among them, only rapid solidification was able to consistently produce over 90% pure MnBi single phase. However, a conventional method such as casting followed by heat treatment is much preferred because of its compatibility with current industrial practice. A recent result by Rao *et al* shows that the conventional cast-anneal method has the potential to achieve 90% single phase material [12, 13].

The Mn–Bi phase diagram shows that in addition to the peritectic reaction, there is a eutectic reaction at 535 K (262 °C), L $\leftrightarrows$ Bi + MnBi. This reaction limits the maximum temperature to which the material can be exposed. While this eutectic temperature is about 62 K higher than the desired operating temperature of 473 K (200 °C), it is rather low for a typical bulk magnet fabrication method such as sintering and hot pressing. In practice, the feedstock powder always contains several per cent of Bi metal as the result of the peritectic reaction. Once the fabrication temperature exceeds

the eutectic temperature at 535 K, Bi and part of the MnBi will transform to Bi rich liquid. Any trace amounts of oxygen may react with the Mn atoms in the liquid resulting in MnO formation. Once MnO is formed, it cannot be reduced even in a hydrogen environment at a temperature <535 K. Excessive Bi will be left behind, causing dissolution of even more MnBi. A thorough understanding of MnBi thermal stability is critical for developing a bulk magnet fabrication method as well as determining the maximum and peak operation temperatures. In this paper, we report our findings on MnBi thermal stability. Our results show that there is a small thermal–mechanical window allowing a bulk MnBi magnet to be fabricated and the resulting magnet is stable up to 473 K (200 °C).

2. Experimental methods

2.1. MnBi powder synthesis and bulk magnet fabrication

MnBi powder was prepared using arc melting followed by grinding, annealing and ball milling. Raw materials, Mn chips and Bi shots, were purchased from Aldrich (SKU 26617 and 556130, respectively). The Mn chips had slight oxidation on the surface, which was removed by polishing with sandpaper. The Mn chips and Bi shots were mixed in approximately 1:1 atomic ratio. The mixture was loaded into the arc-melting furnace, which was subsequently evacuated to 1×10^{-5} Torr. After the first round of arc melting, the ingot was flipped and arc melted again. This flip-and-melt process was repeated 3 times to achieve homogeneity. The obtained ingot was ground into powder using mortar and pestle, and sieved using #60, #200, and #400 mesh screens resulting in particles with average sizes of 250 μm, 75 μm and 37 μm, respectively. The grind–sieve process was carried out in an Argon glove box to avoid oxidization. The obtained powder was annealed at 563 K for 24 h. The obtained powder, sieved by #400 mesh screen, was further ball milled to reduce the particle size to $\sim$5 μm. The $\sim$5 μm powders were aligned using DC or pulsed magnetic field then packed with 35 kpsi isostatic pressure. The obtained green compact was sintered at 530 K for 30 min to achieve 8.4 g cm^{-3} density. Different compositions, heat treatment schedules, ball milling durations, and bulk magnet fabrication processes were found to have large effects on the energy product of the bulk magnet. Investigation of the optimum process is an ongoing effort; the results will be published once the investigation is complete.

2.2. Thermal stability of the MnBi powder

To evaluate the thermal stability of the MnBi powder samples, they were heated to high temperatures in various atmospheres. Samples of four different particle sizes (5, 25, 75, and 250 μm) were heated to two different temperatures (473 and 623 K) under both oxygen containing and oxygen free ambient (air and Ar-2.75%H$_2$) conditions. Thermogravimetric analysis (TGA) and differential scanning calorimetry (DSC) were performed using a Netzsch STA 449C Jupiter system with a ramping rate of 10 K min^{-1} and gas flow rate of 15 ml min^{-1}. Each run used $\sim$50 mg fresh MnBi powder. Magnetic properties of the powder before and after the TGA/DSC analysis were measured

using a Lake Shore 7400 vibrating sample magnetometer for rapid assessment, and using a Quantum Design physical property measurement system (PPMS) with 9 T magnet and vibrating sample magnetometer option for detailed characterization from 10 to 400 K.

2.3. Crystal structure and powder diffraction

Powder diffraction data of the powder before and after the TGA/DSC analysis were collected with a Panalytical X-Pert Bragg–Brentano diffractometer using Cu Kα radiation ($\lambda =$ 1.5416 Å), a graphite post-diffraction monochromator, and variable divergence and anti-scatter slits (illuminated length 10 mm). A 0.05 mm receiving slit was used for increased resolution. Phase proportions and cell parameters were determined by whole-pattern Rietveld fitting using the fundamental-parameters approach implemented in Topas (v4.2, Bruker AXS) and crystal structures from the Inorganic Crystal Structure Database. The focused ion beam technique was used to prepare samples for transmission electron microscopy (TEM), which was used to observe the microstructure of the de-composed powders. Neutron powder diffraction data were collected in the 50–500 K temperature range on the BT-1 high-resolution neutron powder diffractometer at the NIST Center for Neutron Research using a Cu(311) monochromator with wavelength of 1.5403 Å. The intensities were measured with 0.05° scanning step size in the 2θ range 3°–165°. Crystal and magnetic structures were refined with the General Structure Analysis System program [14]. The neutron scattering amplitudes used in refinements were 0.375 and 0.853 ($\times 10^{-12}$ cm) for Mn and Bi, respectively. The sample was sealed in a cylindrical vanadium container filled with He exchange gas.

3. Results and discussion

3.1. Crystal structures of MnBi powder

The obtained powder was analyzed for crystal structure and phase content using neutron powder diffraction. Three phases were used to fit the diffraction pattern; they are MnBi [$P63/mmc$, $a = 4.2909(1)$ Å, $c = 6.1233(9)$ Å], Mn [$I\bar{4}3m$, $a = 8.9211(8)$ Å], and Bi [$R\bar{3}$ mH, $a = 4.5465(3)$ Å, $c = 11.8717(9)$ Å]. The weight fractions of the MnBi, Mn, and Bi phases at 300 K are 91.1%, 5.2%, and 3.7%, respectively. The observed and calculated diffraction patterns are depicted in figure 2.

3.2. Magnetic properties of MnBi powder

Saturation magnetization of the MnBi powder was measured with 9 T applied field while ramping the temperature from 10 to 400 K, then back to 10 K. The *M–T* curve is shown in figure 3. The maximum saturation magnetization, M_S, of the MnBi powder measured 81.2 emu g^{-1} at about 80 K. Beyond 80 K, the M_S decreases monotonically with increasing temperature. From 200 to 400 K, the decrease of M_S is nearly linear, at a rate of about 0.055 emu g^{-1} K^{-1}. The maximum at 80 K can be explained by a simple mean field model. The magnetization
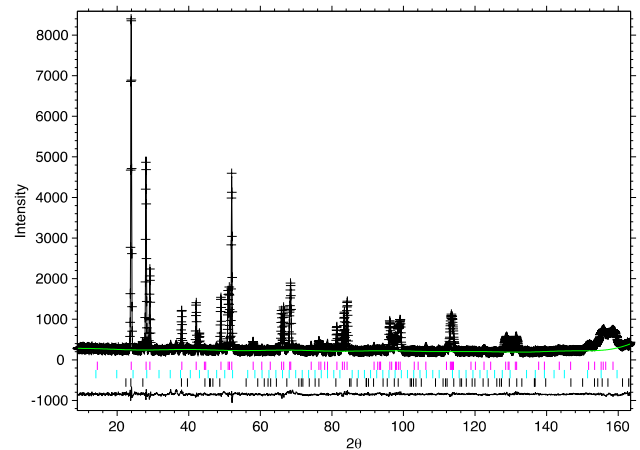
Figure 2. Neutron powder diffraction pattern of the MnBi powder at 300 K.
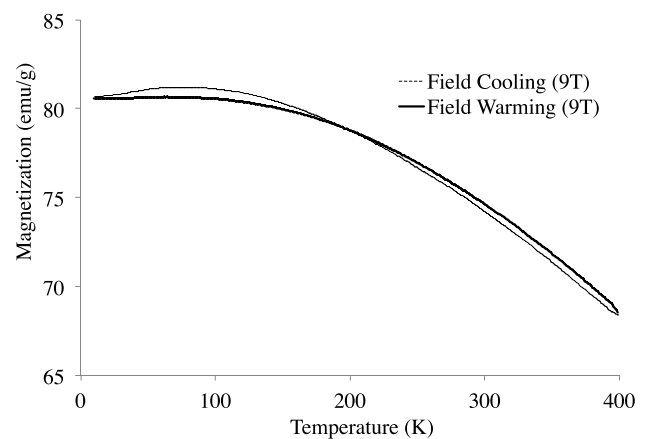
Figure 3. Saturation magnetization of the MnBi powder as a function of temperature. During the temperature ramping the applied magnetic field is kept constant at 9 T.

M of MnBi increases with volume *V*, as we find from density functional theory calculations performed at 0 K. Near 0 K, there are few competing phenomena and the small increase found in the measured $M(V(T))$ is simply due to thermal expansion, $V(T)$. Indeed, a simple model of the magnetization near 0 K yields a Brillouin function behavior with direct $V(T)$ dependence that weakly enhances $M(T)$, which is then quickly overwhelmed by spin thermal disordering resulting in decrease of M at increasing *T*. The phenomenon is general. Mathematically, both the function $M(V)$ and the functional $M(V(T))$ have positive slopes; yet, the thermal disordering of local spins is described by a smooth nonlinear magnetization curve with negative curvature and zero slope at $T = 0$ K; this reduction of magnetization is negligible at low *T* and dominates at higher *T*. From the combination of these two effects, the magnetization of a thermally expanding sample first weakly increases and then decreases with *T*, with an experimentally observed maximum around $T = 80$ K.

Based on the phase fraction results obtained by neutron diffraction (91.1% MnBi) and the magnetization data obtained by PPMS (80.5, 81.2, 74, and 68.5 emu g^{-1} at 10, 80, 300, and 400 K, respectively), the magnetizations of pure MnBi
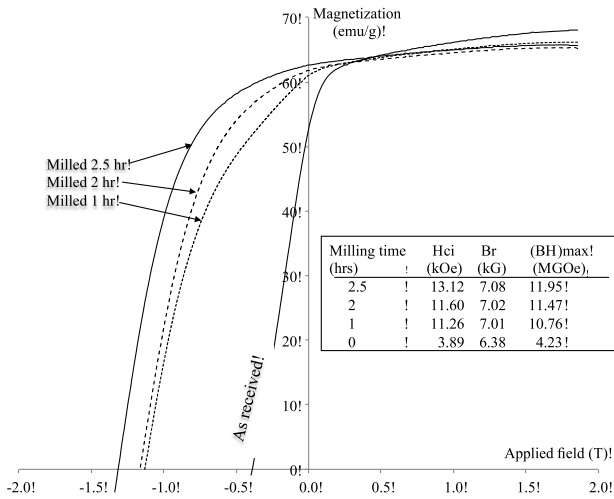
Figure 4. *M–H* curves of the MnBi powders secured with wax after alignment using a 10 T pulsed magnetic field. The curve labeled 'as received' refers to the powder that was sieved using 325 mesh.
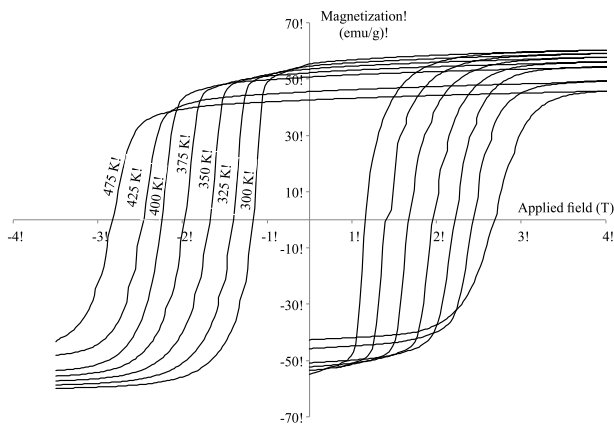
Figure 5. *M–H* curves of a MnBi bulk magnet at various temperatures. The density of the bulk magnet is 8.4 g cm⁻³. The maximum saturation field used was 9 T. Only a portion of each *M–H* curve is depicted.

low temperature phase can be calculated as 88.5, 89.2, 81.3, and 75.3 emu g^{-1} at 10, 80, 300, and 400 K, respectively. This is equivalent to 4.18, 4.24, 3.84, and 3.56 μ_B per MnBi pair at these temperatures. The result agrees with Anderson's 1972 data (4.18 μ_B at 10 K) [15], and is in close agreement with Yang's 2011 data (4.23, 4.1, 3.7 and 3.55 μ_B at 10, 100, 300, and 400 K, respectively) [3]. However, this result has a large discrepancy with Yang's 2013 data (3.99, 3.79, 3.50, and 3.46 μ_B at 10, 100, 300, and 400 K, respectively) [1]. A private discussion with Prof. Yang concluded that the samples' compositions, the facilities used for neutron diffraction, and the data analysis methods are comparable and should not be the causes of the discrepancy. The only possible factor is the sample preparation technique. In our case we used an arc-melting method followed by a long annealing process while Prof. Yang's team used melt-spinning followed by annealing. The rapid solidification process may result in a slightly smaller lattice parameter, which contributes to less magnetic moment per MnBi pair.
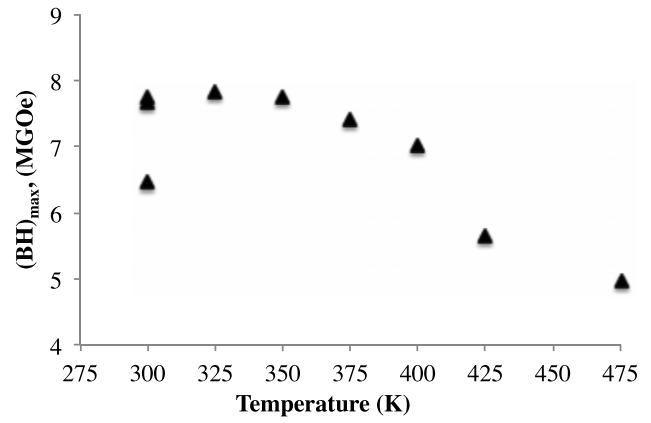
Figure 6. (BH)$_{max}$ of a MnBi bulk magnet at various temperatures.

The ~5 μm powder was aligned using a 10 T pulsed magnetic field and secured with wax. Figure 4 shows the *M–H* curve of the powder–wax mixture at 300 K. The magnetization value shown in the figure is based on the weight with the wax weight subtracted. The wax-bonded powder has the shape of a cylinder with the length/diameter ratio approximately 0.85. A density of 8.9 g cm⁻³ was used to convert emu g^{-1} to kG unit. The energy product of the powder ball milled for 2.5 h is (BH)$_{max}$ = 11.95 MGOe. This is a 28% improvement over the 9 MGOe value reported by Rao *et al* in 2013 [12].

3.3. Magnetic properties of sintered MnBi magnets

Bulk magnets were fabricated using the ~5 μm ball-milled powder. They were first mechanically pressed in a magnetic field, then sintered at 573 K for 60 min. The magnetic properties of the obtained magnets were measured along the alignment direction. Figure 5 shows part of the *M–H* curves at different temperatures. They are plotted in figure 6 as a function of temperature. The (BH)$_{max}$ of the bulk MnBi at 300 K is 7.8 MGOe; this represents a 34% improvement over the 5.8 MGOe previously reported by Hadjipanayis's group [12]. Note that at room temperature, the bulk magnet has about 55 emu g^{-1} remanent magnetization, about 9% less than the 60 emu g^{-1} of the powder. A vacuum oven and a vacuumed quartz tube with backfilled argon were used to minimize oxygen content during hot-pressing and during sintering. However, the oxygen level in the MnBi material still increased from 0.84 wt% to 1.2 wt% after the fabrication. The loss of remanent magnetization is attributed to the oxidization of Mn atoms in the Bi rich liquid, which is formed by the eutectic reaction between Bi and MnBi particles at the fabrication temperature (563 K). This loss of M_r contributes to the 20% loss of (BH)$_{max}$.

3.4. TGA and DSC analysis of MnBi powder

MnBi powders irreversibly gain weight when cycled from room temperature to 623 K in air. The weight gain is attributed to a two-step reaction: first, MnBi and Bi react forming Bi rich liquid; second, Mn atoms in the liquid irreversibly react with oxygen forming MnO, creating more Bi, and causing
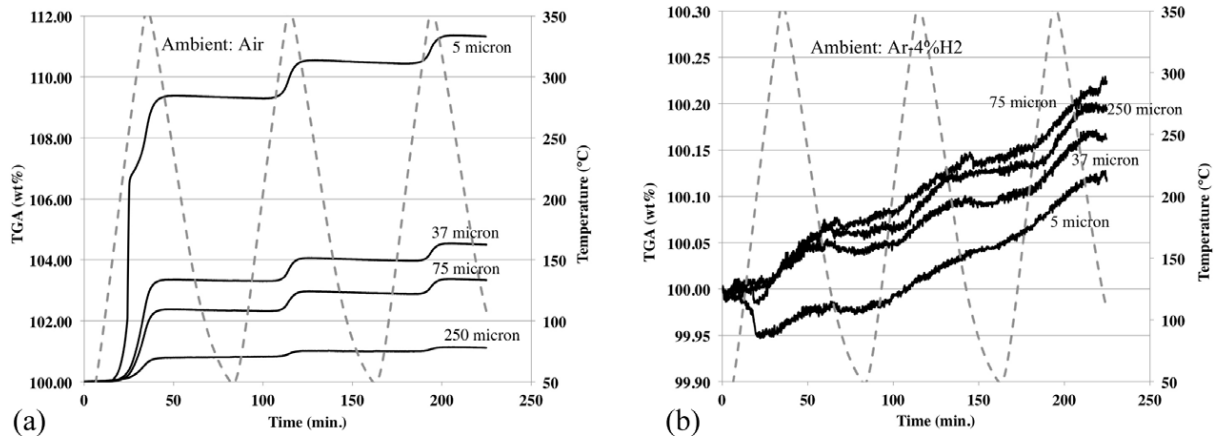
Figure 7. Weight changes of MnBi powders (5, 37, 75, and 250 μm) as a function of temperature in air (a) and in Ar-2.75%H$_2$ (b).

dissolution of more MnBi. The weight gains are inversely proportional to the particle size because of the increasing surface area. Figure 7(a) shows the weight change as a function of temperature when cycled in air 3 times from room temperature to 623 K. The slopes of the weight-gain curves are proportional to the particle sizes, indicating that oxidization rates are faster for smaller particles. While larger particles start to gain weight at about 523 K (250 °C), the 5 μm particle starts to gain weight at about 423 K (150 °C). It appears that the 5 μm particle requires less thermal energy to decompose. It is not clear what causes this 100 K difference. One plausible explanation is that to reduce the particle size from 37 to 5 μm, the particle was ball milled for 50 min, which may have created defects which served as low-energy sites for localized reaction.

Thermal cycling in reducing atmosphere (Ar-2.75%H$_2$) also resulted in weight gain of MnBi particles, but the gains are small. Figure 7(b) shows the weight changes as function of temperature. The 5 μm particle initially loses weight at about 398 K (125 °C). A maximum 0.05% weight loss occurred at about 473 K (200 °C). Since the resolution of the TGA instrument is 0.1 wt%, this 0.05% weight loss could be an error due to slight gas adjustment or organics. It could also be Bi evaporation, even though it occurred at 70 K below its melting temperature, 545 K (271 °C). As the particle sizes get larger, the weight loss becomes smaller, and eventually becomes negligible. After the first 473 K (200 °C) ramp, all particles gain weight at a similar rate. These weight gains are attributed to the trace amount of oxygen in the instrument. The average weight gain for each sample is about 0.1 mg over 225 min. The gas flow rate was 15 ml min^{-1}. The total amount of Ar-2.75%H$_2$ gas used was 3.375 l. For 0.1 mg of oxygen, the corresponding oxygen concentration is about 20 ppb. It is well below the impurity concentration of the Ar-2.75% H$_2$ gas (<10 ppm) used during the test.

DSC curves exhibit multiple overlapping peaks. In consideration of the limited paper length, only 5 and 75 μm DSC curves are shown in figure 8. The numbers, locations, and areas of the DSC peaks were extracted from each DSC curve using the instrument software and are summarized in table 1.

For the particles cycled in air, four peaks per cycle were observed: Peak #1 at ~533 K (260 °C) during the heating run, Peak #2 at ~613 K (340 °C), Peak #3 at ~518 K (250 °C), and Peak #4 at ~453 K (180 °C) during the cooling run. Peaks #1 and #3 match nicely the eutectic reaction L $\leftrightarrows$ Bi + MnBi at 535 K (262 °C). Peak #2 is related to the transition of the MnBi high temperature phase (Mn$_{2.23}$Bi$_{1.88}$, *Pmma*) to the low temperature phase (MnBi, *P*63/*mmc*) [16]. However, Peak #4 is found to be unrelated to any known reaction. Since this peak does not exist when cycled in an Ar-2.75%H$_2$ environment, oxygen must have played a role in this exothermic reaction. Oxidization of Mn and Bi cannot explain the occurrence of this peak because it should not occur only during the cooling run. One possible explanation is the precipitation of Bi after onset solidification of Bi rich liquid, which is the result of MnO formation. When cycled in air, some Mn is removed to form MnO. The remaining material is Bi rich liquid. The investigation of Peak #4 is ongoing.

It is interesting to see that Peak #2, the one corresponding to the transformation of MnBi high temperature phase to low temperature phase, did not exist when the powder was cycled in Ar-2.75%H$_2$, and it did not exist for the 5 μm powder regardless of whether it was in air or in the Ar-2.75%H$_2$ environment. It is not clear why a lack of oxygen can prevent this transformation, or in the 5 μm powder case, why a smaller particle size can prevent the transformation.

For the particles cycled in the Ar-2.75%H$_2$ environment, only two peaks per cycle were observed, Peak #1 at ~533 K (260 °C) during the heating run and Peak #3 at ~523 K (250 °C) during the cooling run. These peak locations match the eutectic reaction at 535 K (262 °C). The magnitudes of the these two peaks in the Ar-2.75%H$_2$ run are much smaller than they are in the air run, implying oxygen promotes the eutectic reaction. Oxygen removes Mn from Bi rich liquid forming MnO, resulting in the remaining material being even more Bi rich. According to the phase diagram shown in figure 1, the eutectic reaction only occurs when excessive Bi is presented with MnBi. When cycled in an Ar-2.75%H$_2$ environment, MnO formation is limited, the amount of Bi available for the

Table 1. Summary of DSC peak location, number and area of the MnBi particles cycled in air and in Ar–H environment. The maximum temperature for each thermal cycle is about 629 K.

Size	Gas	Cyc#	Mass change (wt%)	Peak #1 onset (°C)	Peak #1 Area (J g^{-1})	Peak #2 onset (°C)	Peak #2 area (J g^{-1})	Peak #3 onset (°C)	Peak #4 onset (°C)	Peak #3 and #4 total area (J g^{-1})
5 μm	Air	1	9.3	250	1156.0	—	—	257	180	22.7
		2	1.1	259	−26.7	—	—	257	170	19.6
		3	0.9	260	−22.9	—	—	256	177	16.5
	H$_2$–Ar	1	0.0	256	−4.3	—	—	250	—	4.2
		2	0.1	255	−5.3	—	—	250	—	5.0
		3	0.1	255	−6.3	—	—	250	—	5.5
37 μm	Air	1	3.3	259	−1.8	337	1.2	221	188	17.9
		2	0.7	260	−21.7	338	0.6	241	190	22.9
		3	0.5	259	−25.5	339	0.3	248	187	26.0
	H$_2$–Ar	1	0.0	259	−0.2	—	—	250	—	0.1
		2	0.1	258	−0.5	—	—	258	—	0.3
		3	0.1	259	−0.9	—	—	247	—	0.6
75 μm	Air	1	2.3	260	−2.1	338	2.1	246	184	9.0
		2	0.6	259	−15.9	339	1.6	248	183	12.5
		3	0.4	259	−19.2	339	1.5	252	182	14.7
	H$_2$–Ar	1	0.1	260	−0.5	—	—	248	—	0.2
		2	0.1	259	−0.9	—	—	254	—	0.4
		3	0.1	259	−1.4	—	—	251	—	0.9
250 μm	Air	1	0.8	262	−0.8	341	2.5	223	179	3.2
		2	0.2	261	−4.1	341	3.1	227	178	4.0
		3	0.1	262	−4.8	342	3.4	241	178	4.2
	H$_2$–Ar	1	0.1	262	−0.1	—	—	248	—	0.1
		2	0.1	262	−0.5	—	—	252	—	0.4
		3	0.1	262	−0.8	—	—	254	—	0.8
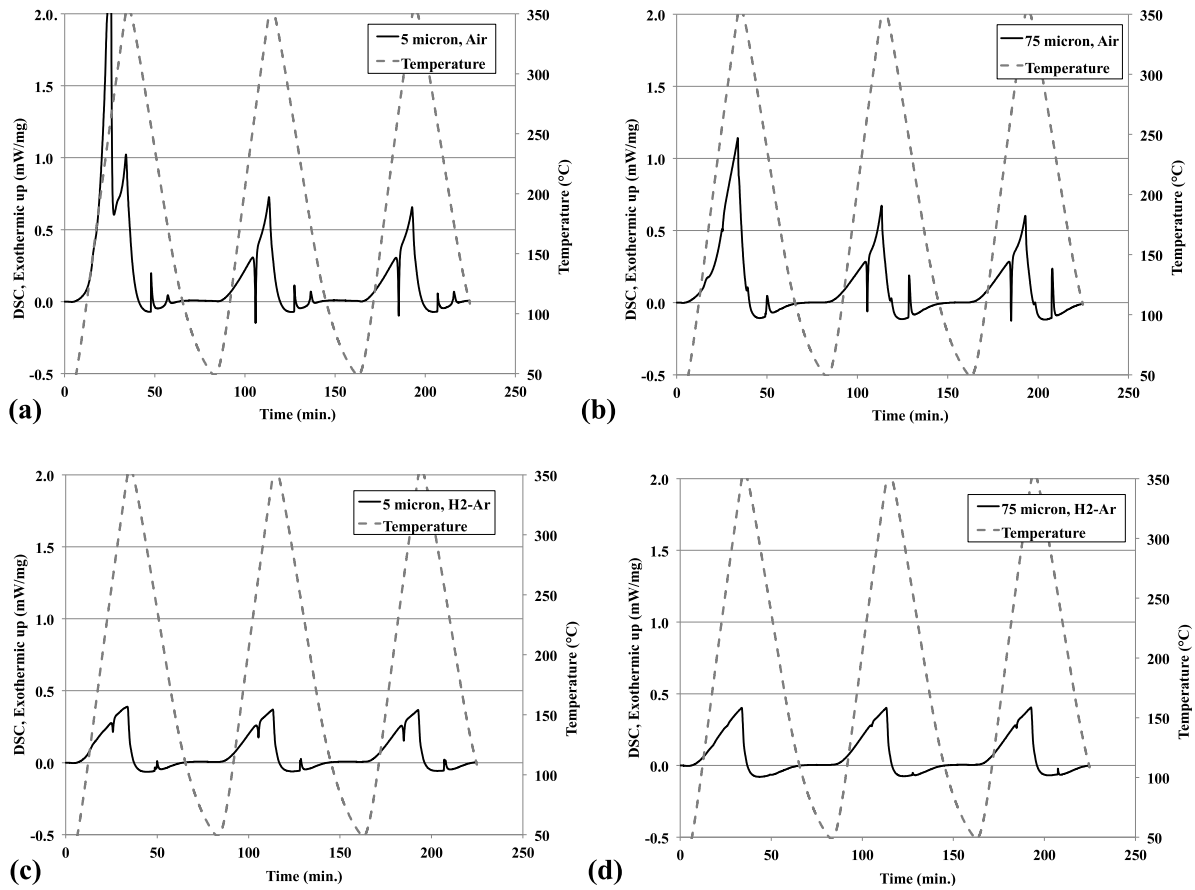
Figure 8. DSC curves of the MnBi powders for the particles of 5 and 75 μm size respectively cycled in air ((a) and (b)), and for the particles of 5 and 75 μm size respectively cycled in Ar-2.75%H_2 ((c) and (d)).

eutectic reaction is less, and the magnitude of the eutectic reaction is smaller.

The 5 μm particles were further investigated for their stability at 473 K. They were cycled from room temperature to 473 K 3 times in air. The TGA and DSC curves are shown in figure 9. Unlike the previous case where the 5 μm particles were cycled to 623 K in air, the weight gain is relatively small and most of the gain occurs at the first ramping. This observation implies that once the particle is passivated, the oxidization will slow down. The DSC curve shows no detectable peaks. This suggests that once a bulk magnet is fabricated and sealed, it can be operated at 473 K without degradation.

3.5. X-ray analysis of the cycled powder

The phase content of the 37 μm particles was analyzed before and after thermally cycling from room temperature to 473 and to 623 K 3 times in air. The lattice parameters and phase fractions of these powders are summarized in table 2. The large increase in Bi and MnO wt% after three thermal cycles to 623 K validates our hypothesis that two reactions occur during the thermal cycling in air: first Bi and part of the MnBi react forming Bi rich liquid, afterward Mn atoms in the liquid are oxidized. In the mean time, the powder cycled to 473 K

in air showed no change in MnBi and MnO wt%. This result supports our previous conclusion that the magnet is stable in air if only exposed to temperatures at or below 473 K.

3.6. Magnetic properties of the cycled powder

A batch of a MnBi powder ($\sim$50 μm particle size) was divided into two portions. Each portion was heated to either 473 K (200 °C) or 623 K (350 °C) in a furnace in air multiple times with the heating rate of 10 K min^{-1}, and kept at the target temperature for 2 min, followed by cooling under a flow of air. The magnetization curves were collected before the first thermal cycle and after the third and the sixth cycles. Figure 10 summarizes the result. It shows that the MnBi samples fully retain their magnetization when cycled to 473 K (200 °C) in air. Heating the powders to 623 K (350 °C) leads to a gradual decrease in magnetization. The reduced magnetization after oxidative thermal cycling at 623 K (350 °C) is attributed to the irreversible oxidation of Mn.

Furthermore, the MnBi powder samples that were subject to DSC/TGA studies were also analyzed by VSM after the thermal analysis was complete. The magnetization data and *M*–*H* curves for the samples of varied particle sizes, which were heated to 623 K (350 °C) in either air or Ar-2.75%H_2, are provided in table 3. As expected, the magnetization decreases
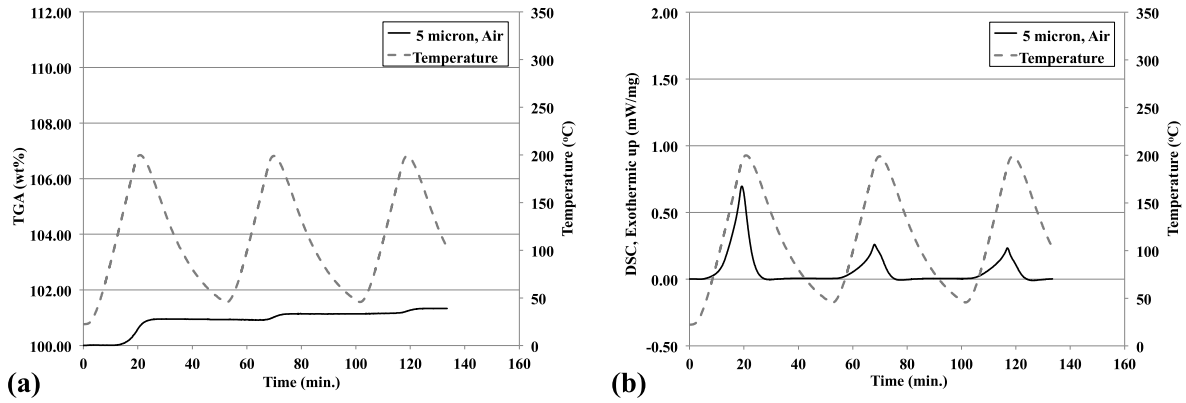
Figure 9. TGA (a) and DSC (b) curves of the MnBi 5 μm particles cycled from room temperature to 473 K (200 °C) in air.

Table 2. Phase ratios and lattice parameters of the MnBi powder as prepared and after cycling 3 times to 623 K and to 423 K in air. The space groups used for the Rietveld refinement are $P63/mmc$ for MnBi, $I\bar{4}3m$ for Mn, $R\bar{3}mH$ for Bi, and $Fm\bar{3}m$ for MnO.

	As prepared	Cycled 3× to 623 K in air	Cycled 3× to 473 K in air
MnBi phase wt%	92.1%	58.9%	92.2%
Lattice parameter:			
a	4.2875	4.2872	4.2873
c	6.1202	6.1213	6.1199
Bi phase wt%	0.7%	23.4%	1.7%
Lattice parameter:			
a	4.544(1)	4.5466(1)	4.544(1)
c	11.899(8)	11.8678(5)	11.903(8)
Mn phase wt%	1.2%	—	—
Lattice parameter:			
a	8.916(2)	—	—
MnO phase wt%	6.1%	17.7%	6.1%
Lattice parameter:			
a	4.444(1)	4.4457(8)	4.443(1)
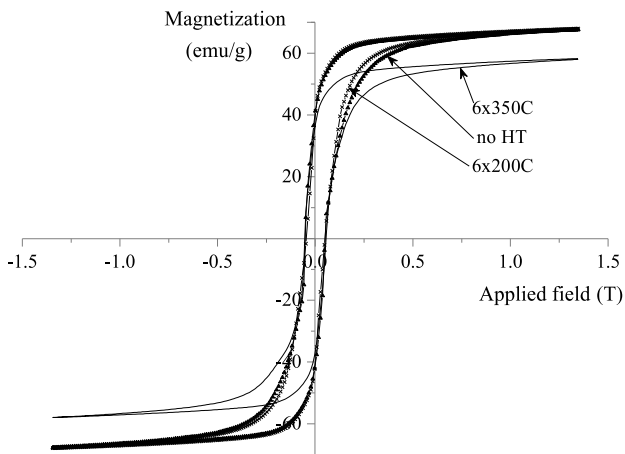
Figure 10. The effect of thermal cycling in air of MnBi powders on the sample magnetization.

Table 3. Dependence of MnBi magnetization (emu g^{-1} at 1 T) on the sample heat treatment conditions and the particle size. Before the heat treatment, the saturation magnetization is about 63 emu g^{-1}.

	Air/350 °C	H$_2$-Ar/350 °C
60 mesh (<250 μm)	50.8	62.3
200 mesh (<74 μm)	22.8	61.2
400 mesh (<37 μm)	13.7	59.7

a decrease in coercivity, whereas the magnetization values change only slightly.

3.7. Microstructure of the bulk MnBi

The starting MnBi powder, as seen in figure 11, appears to have a uniform microstructure, with some larger voids (dark regions) in the middle of the particles. The microstructure observed in the bulk magnet fabricated at 563 K is complicated (figure 12), with significant phase segregation being observed. Figure 12 shows the backscatter electron (BSE) image of the bulk magnet after polishing using a focused ion beam. Toward the center of the particles there is a bright region which is Bi rich, surrounded by a darker region which is Bi poor and

significantly if a sample is heated up to 623 K (350 °C) in air. The decrease of magnetization is inversely proportional to particle size. On the other hand, magnetization of these powders is relatively insensitive to heat treatment under inert or reducing conditions: the decreasing particle size results in
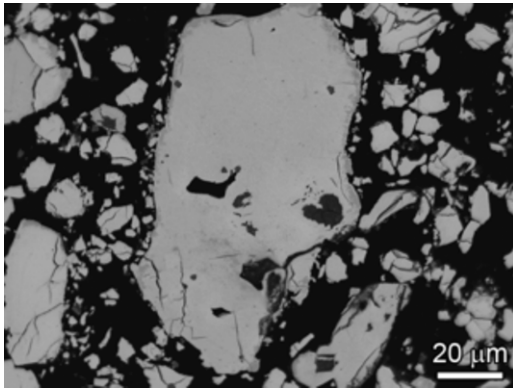
Figure 11. BSE micrographs of the starting MnBi powder at low magnifications.
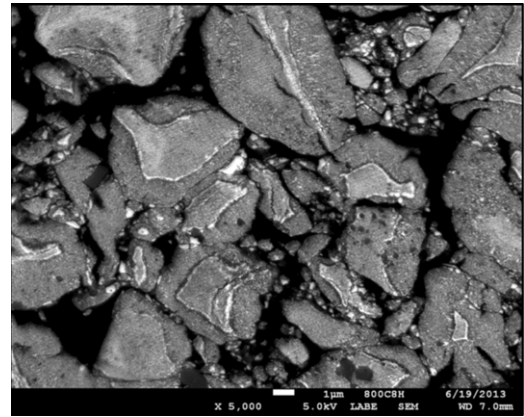
Figure 12. SEM (BSE) of a bulk magnet that was fabricated at 563 K.

Mn rich. The exterior of the particles appears to have brighter grains surrounded by a darker Mn rich continuous phase.

Transmission electron microscopy (TEM) was used to closely examine the interior (core) and exterior (shell) regions. Figure 13 shows a bright field image of the overall microstruc-

ture including the MnBi core and the MnBi shell, separated by a Bi layer (confirmed by diffraction), and figure 14 shows the energy dispersive x-ray spectroscopy (EDS) elemental mapping of the identical region. These images show that the thermal decomposition of MnBi during the warm compaction
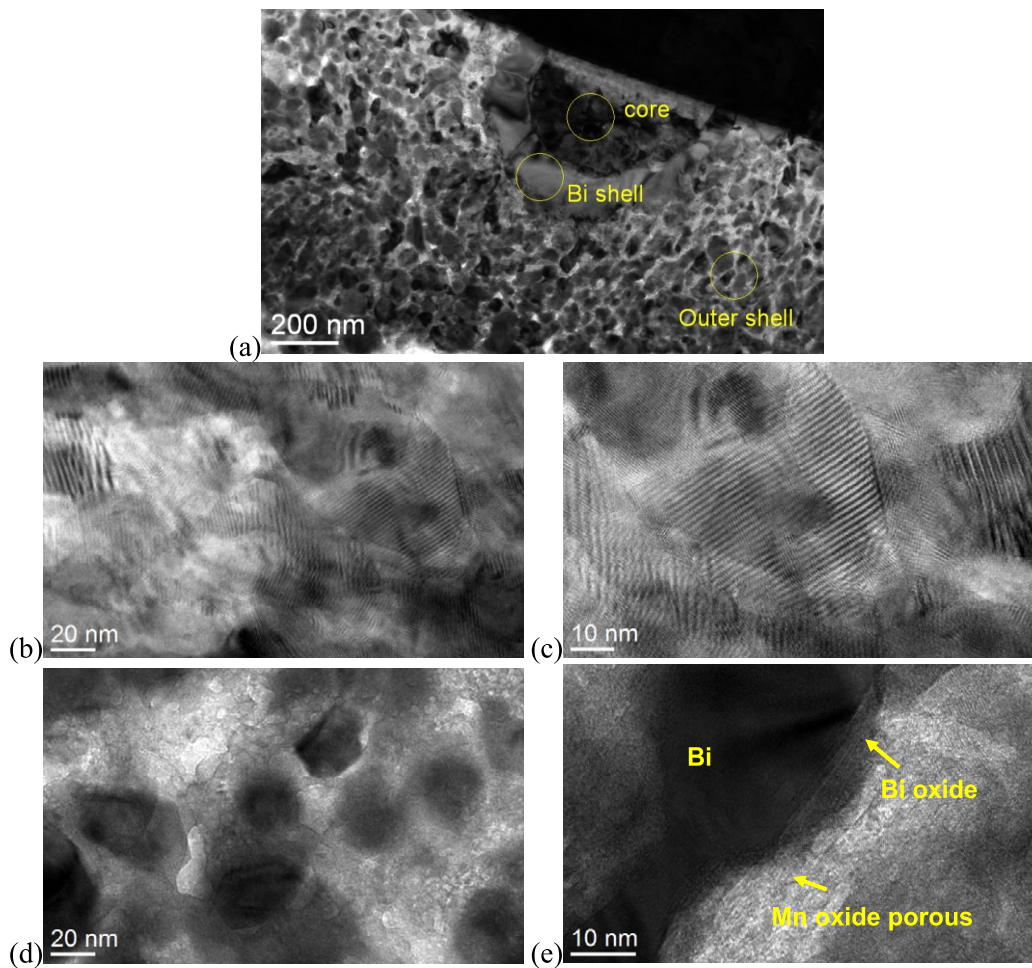
Figure 13. Bright field image of the typical microstructure observed in a bulk magnet hot pressed at 573 K is shown in (a). Brighter regions are manganese rich while darker shades indicate the presence of bismuth. Outer shell regions show Bi metal separated by a nanoporous manganese oxide phase. Bright field and phase contrast TEM images of the core region are shown in (b) and (c). Similar TEM images of outer shell regions are shown in (d) and (e).
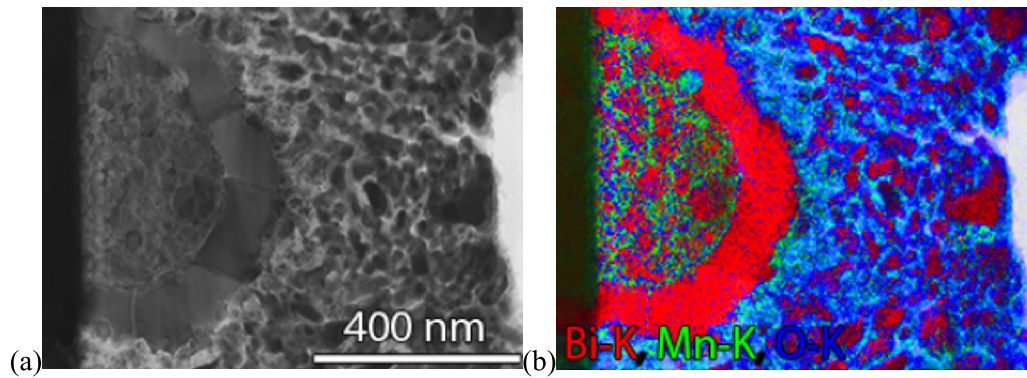
Figure 14. STEM bright field (a) and EDS elemental (b) maps showing the microstructure of the bulk magnet hot pressed at 573 K.

process (563 K for 30 min) can be roughly divided into two stages. In the first stage the outer region of the MnBi grain is transformed to Bi rich liquid phase. The second stage is the Mn atoms in the liquid being oxidized to MnO while Bi is segregated, forming a Bi rich layer. The newly formed Bi layer isolates the core from the outer region where oxygen is relatively abundant. As a result, the warm compaction process will change the originally homogenous MnBi grain to an inhomogeneous structure containing a MnBi core, a Bi shell, and a mixture of MnO, Bi and MnBi.

4. Conclusions

After a year and a half of collective effort, we have gained good understanding of the MnBi compound and its potential as a permanent magnet. The MnBi compound is sensitive to oxygen and to temperature. Oxygen is the driving force for MnBi decomposition when subjected to a temperature higher than 473 K. Once decomposed, the Mn reacts with oxygen forming MnO, causing irreversible loss of magnetic properties. On the other hand, if the fabrication temperature is limited to 473 K and below, the MnBi is stable. Furthermore, if the fabrication process has tight control of oxygen, the fabrication temperature may be increased by a few tens of degrees.

Acknowledgment

References

[1] Yang Y B, Chen X G, Guo S, Yan A R, Huang Q Z, Wu M M, Chen D F, Yang Y C and Yang J B 2013 Temperature dependences of structure and coercivity for melt-spun MnBi compound *J. Magn. Magn. Mater.* **330** 106–10

[2] Yang J B, Yelon W B, James W J, Cai Q, Kornecki M, Roy S, Ali N and l'Heritier P 2002 Crystal structure, magnetic properties and electronic structure of the MnBi intermetallic compound *J. Phys.: Condens. Matter* **14** 6509–19

[3] Yang J B *et al* 2011 Anisotropic nanocrystalline MnBi with high coercivity at high temperature *Appl. Phys. Lett.* **99** 082505

[4] Yang J B, Kamaraju K, Yelon W B, James W J, Cai Q and Bollero A 2001 Magnetic properties of the MnBi intermetallic compound *Appl. Phys. Lett.* **79** 1846–8

[5] Guo X, Chen X, Altounian Z and Stromolsen J O 1992 Magnetic-properties of mnbi prepared by rapid solidification *Phys. Rev.* B **46** 14578–82

[6] Yang Y B *et al* 2012 Preparation and magnetic properties of MnBi *J. Appl. Phys.* **111** 07E312

[7] Okamoto H 1990 *Bi–Mn Phase Diagram* (Materials Park, OH: ASM International)

[8] Yoshida H, Shima T, Takahashi T and Fujimori H 1999 Preparation of highly pure MnBi intermetallic compounds by arc-melting *Mater. Trans. JIM* **40** 455–8

[9] Guo X, Zaluska A, Altounian Z and Stromolsen J O 1990 The formation of single-phase equiatomic MnBi by rapid solidification *J. Mater. Res.* **5** 2646–51

[10] Roberts B W 1956 Neutron diffraction study of the structures and magnetic properties of manganese bismuthide *Phys. Rev.* **104** 607–16

[11] Guo X, Altounian Z and Stromolsen J O 1991 Formation of MnBi ferromagnetic phases through crystallization of the amorphous phase *J. Appl. Phys.* **69** 6067–9

[12] Rao N V R, Gabay A M and Hadjipanayis G C 2013 Anisotropic fully dense MnBi permanent magnet with high energy product and high coercivity at elevated temperatures *J. Phys. D: Appl. Phys.* **46** 062001

[13] Rao N V R, Gabay A M, Li W F and Hadjipanayis G C 2013 Nanostructured bulk MnBi magnets fabricated by hot compaction of cryomilled powders *J. Phys. D: Appl. Phys.* **46** 265001

[14] Larson A C and Von Dreele R B 2000 General structure analysis system (GSAS) *Los Alamos National Laboratory Report* LAUR 86-748

[15] Andresen A F, Engebretsen J E and Refsnes J 1972 Neutron-diffraction investigations on quenched MnBi and MnBi$_{0.9}$Sb$_{0.1}$ *Acta Chem. Scand.* **26** 175

[16] Okamoto H 2000 *Phase Diagrams for Binary Alloys, Desk Handbook* (Materials Park, OH: ASM International)